Low-temperature synthesis of indium tin oxide nanowires as the transparent electrodes for

organic light emitting devices

Low-temperature synthesis of indium tin oxide nanowires as the transparent electrodes for organic light emitting devices

**Yeh Yee Kee[1], Sek Sean Tan[1], Thian Khok Yong[1,4], Chen Hon Nee[1],
Seong Shan Yap[1,5], Teck Yong Tou[1], György Sáfrán[2],
Zsolt Endre Horváth[2], Jason P Moscatello[3] and Yoke Khin Yap[3]**

[1] Faculty of Engineering, Multimedia University, 63100 Cyberjaya, Selangor, Malaysia
[2] Research Institute for Technical Physics and Material Science, Hungarian Academy of Sciences (MFA), Konkoly Thege M. út 29-33, H-1121 Budapest, Hungary
[3] Department of Physics, Michigan Technological University, Houghton, MI 49931, USA

E-mail: tytou@mmu.edu and ykyap@mtu.edu

Abstract

Low-temperature growth of indium tin oxide (ITO) nanowires (NWs) was obtained on catalyst-free amorphous glass substrates at 250 °C by Nd:YAG pulsed-laser deposition. These ITO NWs have branching morphology as grown in Ar ambient. As suggested by scanning electron microscopy (SEM) and high-resolution transmission electron microscopy (HRTEM), our ITO NWs have the tendency to grow vertically outward from the substrate surface, with the (400) plane parallel to the longitudinal axis of the nanowires. These NWs are low in electrical resistivity (1.6×10^{-4} Ω cm) and high in visible transmittance ($\sim$90–96%), and were tested as the electrode for organic light emitting devices (OLEDs). An enhanced current density of $\sim$30 mA cm^{-2} was detected at bias voltages of $\sim$19–21 V with uniform and bright emission. We found that the Hall mobility of these NWs is 2.2–2.7 times higher than that of ITO film, which can be explained by the reduction of Coulomb scattering loss. These results suggested that ITO nanowires are promising for applications in optoelectronic devices including OLED, touch screen displays, and photovoltaic solar cells.

(Some figures may appear in colour only in the online journal)

1. Introduction

The demand for transparent electrode materials has continued to increase due to the increased uses of various optoelectronic devices including light emitting devices (LEDs), touch screen displays, and solar cells. Thin films of indium tin oxide (ITO) have been the most popular option for these applications. However, recent efforts have demonstrated that thin films of nanoscale materials (including single walled carbon nanotubes [1], graphene [2] and ITO nanowires [2, 4]) are good transparent conductors with benefits in cost, materials, and energy efficiency. However, all these reported works involved high growth temperatures [1–4] and required extraction and transfer processes [1, 2]. Thus direct growth of ITO nanowires (NWs) on substrates at low temperatures is particularly attractive for device applications.

In fact, the surface properties of ITO films are expected to affect the characters of optoelectronic devices including

---

[4] Present address: Faculty of Engineering and Science, Universiti Tunku Abdul Rahman, 53300 Kuala Lumpur, Malaysia.
[5] Present address: Institute of Physics, Norwegian University of Science and Technology, 7491 Trondheim, Norway.

the organic LEDs (OLEDs), as the organic films are in contact with the ITO electrode [5, 6]. Very smooth ITO surfaces were thought to be desirable for efficient and stable OLED operations, but this topic is still controversial. There are suggestions that the instability at the organic/electrode interface and the dark spot formation on OLEDs were related to the increased roughness of ITO surfaces [7–9]. However, other reports contradicted this suggestion and claimed that appropriate increases in the ITO film surface roughness by diluted aqua regia surface treatment could greatly enhance the performances of bi-layer OLEDs in terms of current injection levels and electroluminescence outputs [10, 11]. These enhancements are attributed to the increase of contact surface areas and the contact conditions due to the increase in the ITO surface roughness. Furthermore, Yano *et al* [12] and Hashimoto *et al* [13] reported that the presence of a texture or regular relief structures prepared by chemical etching of ITO film surfaces or photolithography improves the performance of polymer/fullerene solar cells. Owing to much larger surface areas offered by ITO nanowires, it is interesting to evaluate them as the electrodes for OLEDs and solar cells.

Synthesis of ITO nanostructures was reported by the co-evaporation method [14], sol electrophoresis with a template [15], the gold catalyst-assisted vapor–liquid–solid growth process [3, 16], electron beam evaporation [17], and pulsed-laser deposition (PLD) with an excimer laser [18]. None of these ITO nanostructures were tested for device applications. Recently, ITO NWs were deposited by molecular beam epitaxy (MBE) with evaporation temperatures of 835–1000 °C [4]. These nanowires were successfully used as the transparent top contact layer for Si/SiGe multiple-quantum-well LEDs. Here we report on low-temperature synthesis of ITO NWs at a substrate temperature of 250 °C by PLD. These ITO NWs were characterized for their crystalline structures, optical transparency, and electrical properties, and then tested as the hole injection anode in OLEDs. We believe that our approach is attractive as it is applicable on substrates with low melting temperatures such as glasses and thus is important for large-scale applications in solar cells, touch screen displays, and OLEDs.

2. Experimental procedures

2.1. PLD deposition of ITO samples

Our ITO films were grown on catalyst-free glass substrates using a *Q*-switched Nd:YAG pulsed laser (EKSPLA, NL301) with an output wavelength of 355 nm [19]. The laser fluence in our experiments is 2.5 J cm^{-2}. The deposition chamber was first evacuated to a base pressure of about 7.0×10^{-4} Pa and Ar gas was admitted at different flow rates to vary the working pressures. The ablation target was a sintered, 2 in diameter disk of ITO with a composition of 90 wt% In$_2$O$_3$ and 10 wt% SnO$_2$ (Target Materials, USA). The ITO target surface was cleaned by ablation for 5 min with an unfocused laser beam before actual deposition of the ITO film. The laser beam was then focused to <1 mm^2 and was scanned over 5×5 mm^2 on the ITO target by an *x–y* motorized mirror.

The deposition distance was fixed at 8 cm perpendicularly opposite the position. The deposition rate was estimated to be about 0.5 nm s^{-1}. The ITO film thickness was about 200 nm, as measured by a stylus profilometer (Perthometer S2, Mahr) and Zygo optical interferometer.

2.2. ITO sample characterization

The electrical resistivity of the ITO films was measured by using both the four-point probe technique and the van der Pauw–Hall effect technique (Hall effect, Lake Shore model 7507 HMS with EM7). The optical transmittance was obtained from the UV–vis–NIR spectrophotometer, which consists of a deuterium–halogen light source (AvaLight-DHc, Avantes) and an optical multichannel analyzer (Ocean Optics) with a spectral range between 200 and 850 nm. The microstructure of the ITO films was obtained with a field-emission scanning electron microscope (FESEM; Hitachi S-4700). The crystalline structures of ITO films were determined by x-ray diffraction (XRD) using a Cu Kα source (wavelength = 1.540 562 Å) and transmission electron microscopy (TEM, JEOL 2010 equipped with a Gatan Tridiem electron energy loss spectrometer, EELS).

2.3. OLED fabrication and characterization

OLEDs were fabricated in a N$_2$-filled glove box inside a clean room. The light emitting layer of the OLED consists of poly(*N*-vinylcarbazole) (PVK) as the host doped with the electron-transport tris(8-hydroxyquinoline) aluminium (III) (Alq$_3$) and the hole-transport *N*,*N*′-bis(3-methylphenyl)-*N*,*N*′-bis-(phenyl)-benzidine (TPD). The host and dopants were dissolved in chloroform at 10 mg ml^{-1} concentration. The ITO samples were patterned into parallel strips by wet etching using diluted aqua regia solution (HNO$_3$ (69%):HCl (37%):H$_2$O of 1:3:4). A 65–75 nm thick layer of (PVK + TPD + Alq$_3$) was spin-coated on top of the patterned ITO. Cross strips of 50 nm aluminium (Al) films are used as the cathode and were thermally evaporated on top of the (PVK + TPD + Alq$_3$) layer at 5.3×10^{-4} Pa. The mutually orthogonal overlapping areas between the ITO electrode and the Al strips formed the OLED, each with an area of 0.075 cm^2. A control sample of OLED was fabricated using the commercial ITO film ($\rho \sim 28$ Ω/sq, $T \sim 90\%$). The current density versus applied voltage (*J–V*) characteristic and the electroluminescence or brightness of OLEDs was measured, respectively, using a source-meter (Keithley 238 *I–V*) and an optical power meter with a silicon photo-detector (Oriel Instruments, model 70260).

3. Results and discussion

The XRD patterns of ITO samples grown in Ar are shown in figure 1. The inset pictures are the SEM surface images of the corresponding ITO samples. As shown in figure 1, XRD diffraction patterns indicate that all the ITO samples have cubic bixbyite structure of In$_2$O$_3$ [20]. There are four
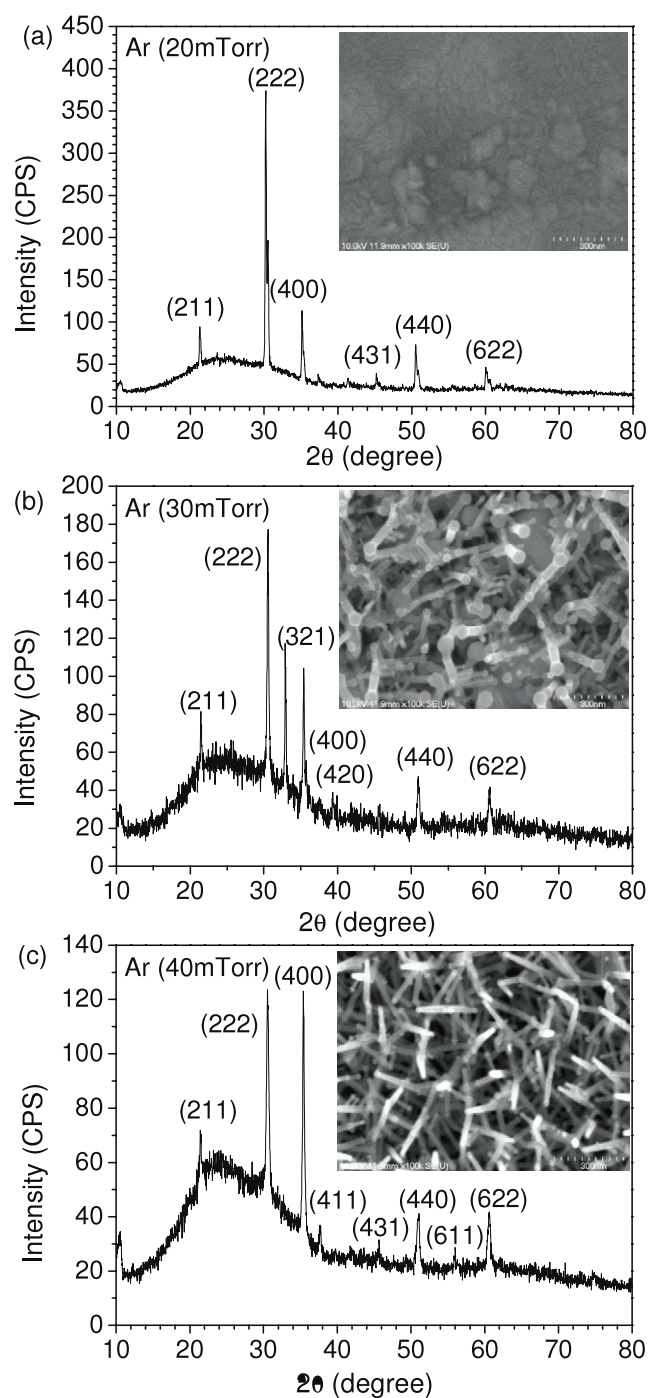
Figure 1. XRD and SEM of ITO samples grown in Ar ambient of (a) 20 mTorr, (b) 30 mTorr, and (c) 40 mTorr.

major diffraction peaks corresponding to (222), (400), (440) and (622) orientations. At the lower deposition pressure of 20 mTorr Ar, the ITO sample grown has polycrystalline films (figure 1(a)). As the deposition pressure increases to 30 mTorr, ITO nanowires are formed (figure 1(b)). At higher deposition pressure of 40 mTorr, the synthesized ITO nanowires (diameter < 50 nm) are compactly knitted as shown in figure 1(c). The nanowires are longer and more uniform in size as compared to those synthesized at lower pressure. Although the nanowires are not perfectly oriented

on the substrate, they have a tendency to grow perpendicularly above the substrate with branches. We also noticed some differences in the XRD spectra between samples shown in figure 1, which is likely due to the random orientation of the polycrystals (figure 1(a)) and the nanowires (figures 1(b) and (c)).

Figure 2 shows the cross-sectional TEM images of an ITO sample grown at 40 mTorr Ar pressure. According to the TEM image (a) and the indium mapping by EELS (b), these ITO nanowire films consists of two different morphologies. Immediately above the glass substrate (upper left corner of figure 2(a)), there is a 50–80 nm thick layer of globular structures with a grain size of ∼20–50 nm. This is followed by the growth of branching ITO nanowires. The 'trunks' of the nanowires are ∼20 nm in diameter and ∼700–800 nm in length. The 'branches' of the nanowires are slightly smaller in diameter (∼15 nm). As shown in figure 2(b), the indium map is identical to the TEM image, indicating uniform distribution of indium atoms over the entire ITO nanowires. The magnified TEM image in figure 2(c) shows the irregular surface morphology of the ITO nanowires. An area of the nanowire (marked by the rectangle) is magnified in figure 2(d). The high-resolution image and its fast Fourier transform (inset) represent that the (400) lattice fringes of 0.256 nm period are parallel to the longitudinal axis of the nanowire. This means that our nanowires are grown along the (400) plane. This structural feature together with the branching features explains the strong (400) XRD peak detected from this sample (40 mTorr) as compared to that deposited at lower Ar pressures as shown in figure 1.

Prior to the use of these ITO samples for OLEDs, we characterized their optical and electrical properties. Figure 3 shows the typical optical transmittance (%) for ITO films grown in Ar, and the commercial ITO film. All the ITO samples had an optical transmittance ∼90–96% in the visible range (400–800 nm). The nanowire samples grown in Ar seems to have higher transmittance at the ∼300–400 nm range but lower transmittance at the ∼420–600 nm range than the commercial sample. Meanwhile, table 1 summarizes the electrical resistivity, carrier density, and Hall mobility of a commercial ITO sample as compared to the ITO NW samples grown in Ar ambient at different deposition pressures. It is observed that there exists an optimum pressure for the lowest ITO resistivity. The lowest resistivity obtained for our ITO NW samples grown in Ar is comparable to the commercial ITO.

It is interesting to observe that the NW samples have much higher charge carrier mobility (2.2- to 2.7-fold) than the commercial ITO film. Despite the fact that NWs prepared by PLD have lower carrier densities, their much higher mobility has contributed to the low resistivity, comparable to that of the ITO film. We have examined the XRD spectra of the commercial sample and found that the signal is relatively weak and noisy (not shown here). This may be due to the small thickness of the thin film. We can only resolve the (400) peak, and fitted it with a single Gaussian peak with full width at half maximum (FWHM) of 0.4367°. The FWHMs for the nanowire samples deposited at 30 mTorr and 40 mTorr
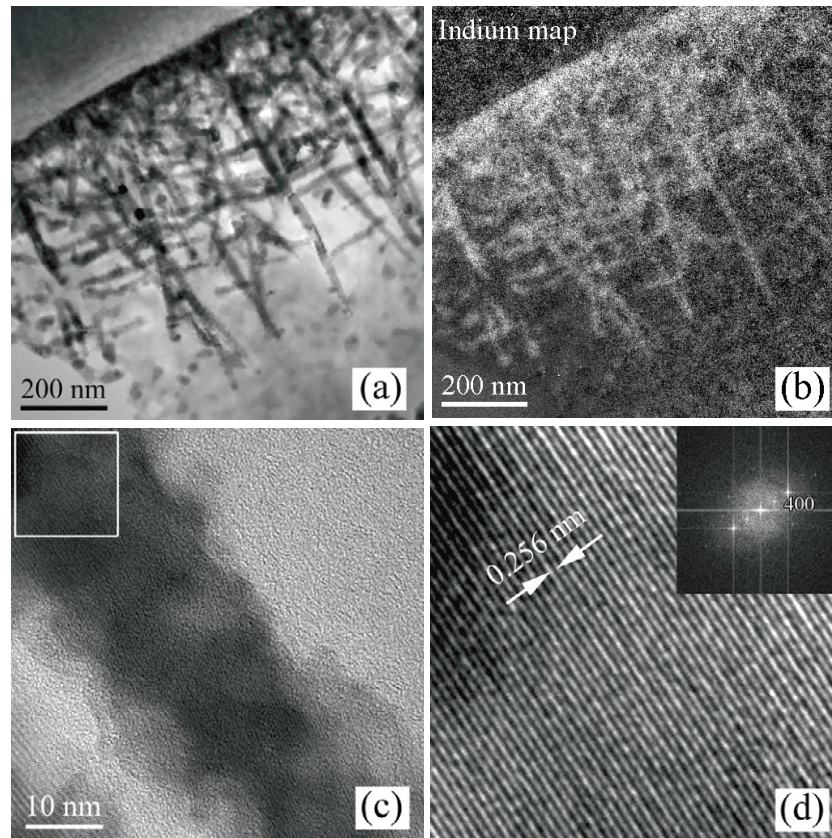
Figure 2. (a) TEM of an ITO sample grown in 40 mTorr Ar and (b) the corresponding EELS map for indium. (c), (d) HRTEM and fast Fourier transform (inset in (d)) of a nanowire.
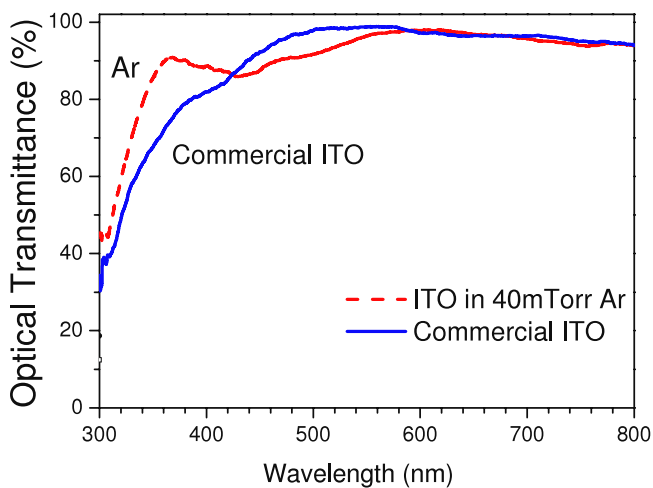

Figure 3. Optical transmission spectra of commercial ITO and ITO samples grown in Ar and He background gases.

Table 1. Resistivity, carrier density and Hall mobility of commercial ITO films and ITO nanowires grown in Ar ambient.

ITO samples	Resistivity ($\times 10^{-4}$ Ω cm)	Carrier density ($\times 10^{20}$ cm^{-3})	Hall mobility (cm^2 V^{-1} s^{-1})
Commercial ITO	1.97	18.7	16.6
Ar (30 mTorr, 250 °C)	1.61	10.5	36.7
Ar (40 mTorr, 250 °C)	2.09	6.65	44.9

are 0.239 08° and 0.297 78°, respectively. Since the XRD peak width is inversely proportional to crystallite size [20], it is clear that nanowires have better crystallinity and thus offer higher mobilities due to reduced electron scattering at the crystallite boundaries/defects. The crystallite sizes (L) were estimated using the Scherrer equation, $L = K\lambda / B \cos\theta$, where K is the Scherrer constant ($\sim$0.94 assuming spherical crystallites), λ is the wavelength of our x-ray source, B is the broadening (FWHM in radians) of the (400) peak in this case, and θ is the Bragg angle of the (400) peak. As estimated, $L = 20.0$ nm, 36.4 nm, and 29.2 nm, respectively, for the ITO film and ITO nanowires deposited at 30 mTorr and 40 Torr, respectively. However, it is interesting to see that the nanowire sample deposited at 40 mTorr has higher mobility than the sample prepared at 30 mTorr although the latter has narrower (400) peak and larger crystallite sizes. This can be explained by Coulomb scattering as described hereafter.

In fact, such an enhanced mobility at the nanoscale has been recently detected in nanoscale silicon-on-insulator (SOI) [21]. The reason for such an enhancement is the
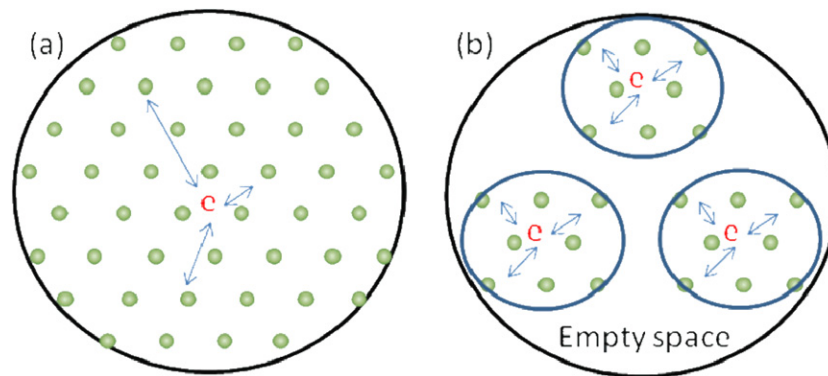
Figure 4. Schematic representation of Coulomb scatterings in (a) ITO film and (b) nanowire samples as viewed from the top of the samples.

reduction of scattering loss from surrounding Coulomb centers. As for our case, this situation can be explained based on a two-dimensional Coulomb scattering model as schematically illustrated in figure 4. As shown in figure 4(a), the mobility of a conducting electron in the ITO film is affected by both long- and short-range interactions with the surrounding lattice, both from the electron clouds and atoms with positive ionic cores. In this case, the total Coulomb force encountered by the conducting electron is $F = \sum K(eQ_i/r_i^2)$, as we assume an instantaneous electrostatic condition, where K is the electrostatic constant, e is the charge of the conducting electron in consideration, Q_i is the charge of the interacting charge i, and r_i is the distance between the electron and the charge i. This means that a conducting electron will be scattered by various Coulomb centers at both short and long ranges. On the other hand, the mobility of a conducting electron in the ITO NW sample is affected by smaller number of scattering centers as shown in figure 4(b). As now there are no atoms, ions, and electrons between NWs (empty space), and the long-range scattering centers are now eliminated, the total number of lattice scattering centers and the total interactive force are reduced. This has led to higher mobility in the NW samples as compared to that in the ITO film. It is also noted that the diameters of nanowires deposited at 30 mTorr are larger than those deposited at 40 mTorr (see insets of figures 1(b) and (c)). This means that the former are less porous (denser in space) and have more long-range interactions. Thus the sample deposited at 30 mTorr has lower mobility that deposited at 40 mTorr as shown in table 1.

In order to investigate the effect of the ITO surface morphology on the OLED performance, ITO NWs grown in Ar with the lowest resistivity were used as an anode for fabrication OLEDs with ITO/PVL + TPD + Alq3/Al configuration. Figures 5(a) and (b), respectively, show the current density (J) versus bias voltage (V) characteristic of OLEDs fabricated by an NW sample and a commercial ITO film. All the data points represent an average value for three to five individual OLEDs fabricated on the same ITO sample. The threshold voltage of these OLEDs was lower than that of devices fabricated by the commercial ITO film. The enhancement in current density of the NW sample is as high as $\sim$30 mA cm^{-2} at $\sim$19–21 V. As shown in figure 5(b), uniform and bright emission was detected from the NW
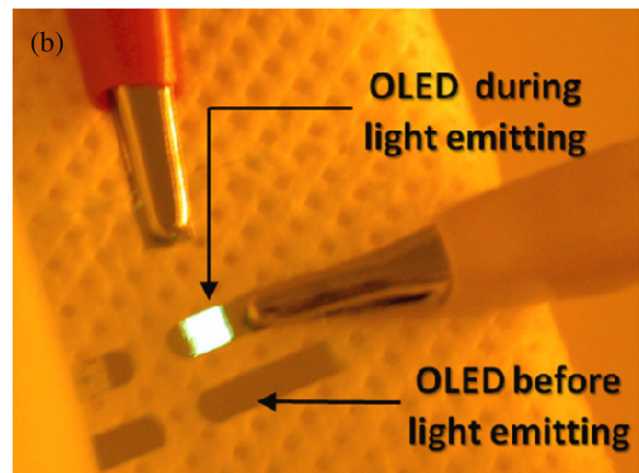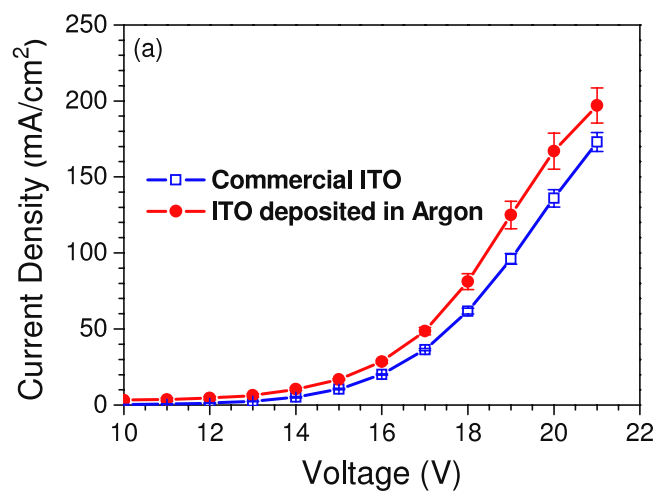

Figure 5. Comparison of (a) current density–bias voltage (J–V) characteristic and (b) images of the nanowire-based OLED devices before and during emission.

samples. Tentatively, we attribute the lower threshold voltage and enhanced current density of the NW device to higher contact area between the NWs and the organic films, which leads to higher charge injection. This is consistent with the interpretation reported by Haque *et al*, where nanostructured TiO$_2$ films were shown to increase the charge injection in a multilayer polymer LED [22].

4. Conclusion

ITO NWs were successfully synthesized on glass substrates by Nd:YAG pulsed-laser deposition at 250 °C in Ar ambient. Rational control of the growth process allows the fabrication of ITO NWs with electrical and optical properties comparable to commercial ITO films. Furthermore, ITO NWs offer higher Hall mobility than the commercial ITO films. Larger contact areas and higher charge injection were introduced on OLEDs fabricated using the ITO NWs, which led to higher emission current density.

References

[1] Wu Z, Chen Z, Du X, Logan J M, Sippel J, Nikolou M, Kamaras K, Reynolds J R, Tanner D B, Hebard A F and Rinzler A G 2004 Transparent, conductive carbon nanotube films *Science* **305** 1273–6

[2] Wang X, Zhi L and Mülle K 2008 Transparent conductive graphene electrodes for dye-sensitized solar cells *Nano Lett.* **8** 323–7

[3] Wan Q, Dattoli E N, Fung W Y, Guo W, Chen Y, Pan X and Lu W 2006 High-performance transparent conducting oxide nanowires *Nano Lett.* **6** 2909–15

[4] O'Dwyer C, Szachowicz M, Visimberga G, Lavayen V, Newcomb S B and Sotomayor Torres C M 2009 Bottom-up growth of fully transparent contact layers of indium tin oxide nanowires for light-emitting devices *Nature Nanotechnol.* **4** 239–44

[5] Sato Y, Ichinosawa S and Kanai H 1998 Operation characteristics and degradation of organic electroluminescent devices *IEEE J. Sel. Top. Quantum Electron.* **4** 40–8

[6] Kim J S, Granström M, Friend R H, Johansson N, Salaneck W R, Daik R, Feast W J and Cacialli F 1998 Indium–tin oxide treatments for single- and double-layer polymeric light-emitting diodes: the relation between the anode physical, chemical, and morphological properties and the device performance *J. Appl. Phys.* **84** 6859–70

[7] Do L, Hwang D, Chu H, Kim S, Lee J, Park H and Zyung T 2000 The initial state of dark spot in degradation of polymer lighting-emitting diodes *Synth. Met.* **111/112** 249–51

[8] Jonda Ch, Mayer A B R, Stolz U, Elschner A and Karbach A 2000 Surface roughness effects and their influence on the degradation of organic light emitting devices *J. Mater. Sci.* **35** 5645–51

[9] Tak Y, Kim K, Park H, Lee K and Lee J 2002 Criteria for ITO (indium–tin-oxide) thin film as the bottom electrode of an orgnai light emitting diode *Thin Solid Films* **411** 12–6

[10] Li F, Tang H, Shinar J, Resto O and Weisz S Z 1997 Effects of aquaregia treatment of indium–tin-oxide substrates on the behavior of double layered organic light-emitting diodes *Appl. Phys. Lett.* **70** 2741–3

[11] Wantz G, Hirsch L, Huby N, Vignau L, Silvain J F, Barriére A S and Parneix J P 2005 Correlation between the indium tin oxide morphology and the performances of polymer light-emitting diodes *Thin Solid Films* **485** 247–51

[12] Yano H, Kouro D, Sasaki N and Muramatsu S 2009 Improvement of polymer/fullerene solar cells by controlling geometry of the ITO substrate surface *Sol. Energy Mater. Sol. Cells* **93** 976–9

[13] Hashimoto Y, Umeda T, Mizukami H, Fujii A, Ozaki M and Yoshino K 2005 Effect of indium–tin oxide surface micromodification and improvement of long-wavelength sensitivity on photovoltaic properties of photovoltaic cell with conducting polymer/C_{60} interpenetrating heterostructure *Japan. J. Appl. Phys.* **44** 1978–81

[14] Wan Q, Song Z T, Feng S L and Wang T H 2004 Single-crytalline tin-doped whiskers: synthesis and characterization *Appl. Phys. Lett.* **82** 4759–61

[15] Limmer S J, Cruz S V and Cao G C 2004 Films and nanorods of transparent conducting oxide ITO by a citric acid sol route *Appl. Phys.* A **79** 421–4

[16] Nguyen P, Vaddiraju S and Meyyappan M 2006 Indium and tin oxide nanowires by vapor–liquid–solid growth technique *J. Electron. Mater.* **35** 200–6

[17] Pokaipisit A, Udomkan N and Limsuwan P 2006 Nanostructure and properties of indium tin oxide (ITO) films produced by electron beam evaporation *Mod. Phys. Lett.* B **20** 1049–58

[18] Savu R and Joanni E 2006 Low-temperature, self–nucleated growth of indium–tin oxide nanostructures by pulsed-laser deposition on amorphous substrates *Scr. Mater.* **55** 979–81

[19] Yong T K, Yap S S, Sáfrán G and Tou T Y 2007 Pulsed Nd:YAG laser depositions of ITO and DLC films for OLED applications *Appl. Surf. Sci.* **253** 4955–9

[20] Langford J I and Wilson A J C 1978 Scherrer after sixty years: a survey and some new results in the determination of crystallite sise *J. Appl. Crystallogr.* **11** 102–13

[21] Kadotani N, Takahashi T, Ohashi T, Oda S and Uchida K 2011 Electron mobility enhancement in nanoscale silicon-on-insulator diffusion layers with high doping concentration of greater than 1×10^{18} cm^{-3} and silicon-on-insulator thickness of less than 10 nm *J. Appl. Phys.* **110** 034502

[22] Haque S A, Koops S, Tokmoldin N, Durrant J R, Huang J, Bradley D D C and Palomares E 2007 *Adv. Mater.* **19** 683–7